Hardening of the soft phonon in bulk $SrTiO_3$ interfaced with $LaAlO_3$ and $SrRuO_3$

A. Nucara,[1] M. Ortolani,[2] L. Baldassarre,[1] W. S. Mohamed,[2] U. Schade,[3] P. P. Aurino,[4] A. Kalaboukhov,[4] D. Winkler,[4] A. Khare,[5] F. Miletto Granozio,[5] and P. Calvani[1]

[1]*CNR-SPIN and Dipartimento di Fisica, Università di Roma "La Sapienza", P.le A. Moro 2, I-00185 Roma, Italy*

[2]*Dipartimento di Fisica, Università di Roma "La Sapienza", P.le A. Moro 2, I-00185 Roma, Italy*

[3]*Helmholtz Zentrum Berlin Mat & Energie GmbH, Methods Mat Dev, D-12489 Berlin, Germany*

[4]*Dept. of Microtechnology & Nanoscience, Chalmers University, S-41296 Gothenburg, Sweden*

[5]*CNR-SPIN UOS Napoli, Complesso Universitario di Monte Sant'Angelo, Via Cinthia I-80126, Napoli, Italy*

(Received 3 December 2015; revised manuscript received 1 June 2016; published 14 June 2016)

The low-temperature softening of the TO1 phonon of $SrTiO_3$ (STO), which determines its incipient ferroelectricity, is known to be partially hindered either in the bulk under strong electric fields, or in thin STO films. Here we show, by terahertz (THz) reflectivity measurements, that a similar effect is produced in bulk STO and at zero static field by ultrathin metallic films on its surface, like a 10-nm-thick film of $SrRuO_3$ (SRO), or the two-dimensional electron system (2DES) present at the interface with $LaAlO_3$. In SRO/STO, the observed hardening is well explained by the depolarizing action of the SRO free electrons which follow adiabatically the ion motion. In LAO/STO, a weaker TO1 hardening could be detected by patterning the 2DES in the form of microstripes and using a polarized THz field parallel ($\vec{E}_\parallel$) or orthogonal ($\vec{E}_\perp$) to the stripes. At 10 K, when TO1 is excited together with the free electrons by $\vec{E}_\parallel$, its absorbance is harder by about 7 cm^{-1} than that measured when TO1 is coupled to the plasmon-polariton confined within the stripes, being excited by $\vec{E}_\perp$.

DOI: 10.1103/PhysRevB.93.224103

I. INTRODUCTION

The phenomenon of incipient ferroelectricity [1] in $SrTiO_3$ (STO) has been widely investigated in the past decades, both for its intrinsic interest, and for the possible applications to oxide-based electronic devices [2,3]. With a cubic structure (space group O_h) which becomes tetragonal (D_{4h}) below [4] $T_c = 105$ K, bulk STO would enter a ferroelectric phase at [5] $T_c \simeq 37$ K if the transition were not prevented by the quantum fluctuations of the ion motion [6]. For this reason STO is also called a "quantum paraelectric" material. Its relative permittivity, namely, the real part $\epsilon_1(0)$ of the dielectric function $\tilde{\epsilon}(\omega)$ at $\omega = 0$, increases from about 300 at 300 K to more than 20 000, in best samples, at 4 K [7]. Correspondingly, the center-zone infrared frequency Ω_{TO1} of the lowest-energy transverse mode (TO1) (i.e., the Ti-O cage anharmonic vibration with respect to the Sr lattice) decreases [8] from 90 cm^{-1} at 300 K to [9] 18 cm^{-1} at 5 K [10] in agreement with the Lyddane-Sachs-Teller (LST) relation

$$\epsilon_1(0)/\epsilon_\infty = \prod_{j=1}^{n} [\Omega_{LOj}^2/\Omega_{TOj}^2], \tag{1}$$

where ϵ_∞ is $\epsilon_1(\omega)$ at $\omega \gg \Omega_{TOj}$, and $n = 3$ above T_c, $n = 4$ below T_c. Indeed, both Ω_{TO2} and Ω_{TO3}, as well as the longitudinal phonon frequencies Ω_{LOj}, are weakly dependent on temperature. The TO1 softening is sensitive to an external static electric field $\vec{E}_0$, applied to STO by a metal electrode: in bulk STO at 90 K, a field of 40 kV/cm increased Ω_{TO1} by about 2 cm^{-1} with respect to zero field, for $\vec{E}_0$ orthogonal to the STO surface, by 11 cm^{-1} for $\vec{E}_0$ parallel to the surface [12]. This effect was attributed to the depolarizing action of $\vec{E}_0$, which was shown to reduce the anharmonicity of the ionic potential [12]. In another experiment [13], aimed at confirming the validity of Eq. (1) in thin STO films, the authors interposed between a 2-μm-thick STO film and the STO substrate a 0.35-μm-thick film of $SrRuO_3$ (SRO), to shield the substrate from terahertz (THz) radiation. They observed that Ω_{TO1} hardened by more than 40 cm^{-1} at low T, and attributed this huge hardening, recently confirmed by further experiments [14], to strain and/or crystal defects in the STO film. We wondered instead if the SRO might have a role in this intriguing effect, namely if, and how, a thin metal layer may affect the anharmonicity of the ionic motion, and therefore the dielectric properties of STO, even in the absence of static fields. We have then measured in the THz range the reflectivity of bulk STO both under a film of SRO, so thin (10 nm) as to be semitransparent to THz radiation, and under films of $LaAlO_3$ (LAO), with and without the two-dimensional electron system (2DES) which spontaneously forms at the interface with STO [15,16] when the LAO thickness d is larger than $d_c = 4$ unit cells. The resulting 2DES has the same thickness as SRO ($\approx$10 nm) [17]. Both in SRO/STO and in LAO/STO we have measured an appreciable hardening of the TO1 mode, but in the case of 2DES the effect is weaker than under a conventional metal film and its detection required a more refined experimental procedure.

II. EXPERIMENT

Four films were deposited on crystalline, TiO_2 terminated, STO substrates by pulsed laser deposition (PLD) (see Table I). The three $LaAlO_3$ films (S1, S2, S4) were grown [18] at a substrate temperature of 800 °C and under an oxygen pressure of 10^{-4} mbar, and further annealed for one hour at 600 °C and 500 mbar. They all were crystalline, had a thickness of 10 cells ($d \simeq 4$ nm) and a conducting 2DES at the interface. The sheet resistance of one of them is shown in Fig. 1. Sample S1 was then exposed to an Ar^+ beam [18] for 5 min at a beam energy of 150 eV, in order to erase the 2DES, while another one (S2) was kept intact. The 2DES of the third LAO/STO sample (S4) was patterned by the ion beam in the

TABLE I. Characteristics of the four samples measured in the present work; see text.

Name	Interface	d (nm)	Ion etching	Outcome
S1	LAO/STO	4	Full surface	No 2DES
S2	LAO/STO	4	None	Full 2DES
S3	SRO/STO	10	None	Metallic layer
S4	LAO/STO	4	Lithographic	2DES stripes

form of conducting stripes of width $W = 2.4$ μm and period $P = 4.0$ μm, separated by insulating stripes. Figure 2 shows the image, taken with an atomic force microscope (AFM), of sample S4 (a), together with its height profile (b) along the line shown in (a). The SRO/STO sample S3 was instead obtained by depositing on strontium titanate a 10-nm-thick metallic film of $SrRuO_3$ (SRO). As shown in Fig. 3, this film exhibited a ferromagnetic transition at $\simeq$ 140 K and a metallic dc resistivity ρ which attained 8×10^{-5} Ω cm at 10 K. The reflectivity $R(\omega)$ of all films was measured at exactly normal incidence [19] by a Michelson interferometer and a bolometer working at 4.2 K, also using the infrared synchrotron radiation of the IRIS beamline at BESSY-II. The samples were mounted on the cold finger of a He-flow cryostat, and thermoregulated within $\pm$2 K. The reference was an Au mirror aligned parallel to the sample by a laser beam. The reproducibility in $R(\omega)$ was typically $\pm$0.5% rms [19].

III. RESULTS AND DISCUSSION

A. Dielectric function of the LAO/STO system

The normal-incidence reflectivity of sample S1 (LAO/STO without 2DES) is shown for reference in Fig. 4(a), and that of S2 (LAO/STO with 2DES) is reported in Fig. 4(b). No spectral feature that might be attributed to the 4-nm-thick LAO film is observed in the $R(\omega)$ of S1 and S2. One can distinguish instead, besides the strong contributions of the TO1 and TO2

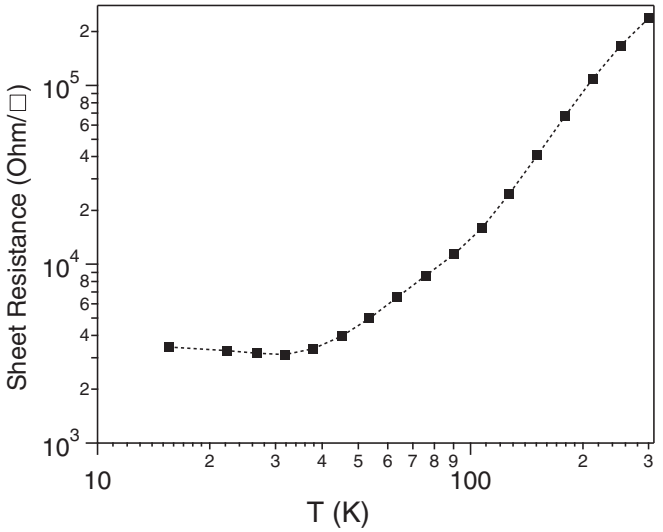

FIG. 1. Sheet resistance of LAO/STO sample S4, prior to patterning, as a function of temperature.

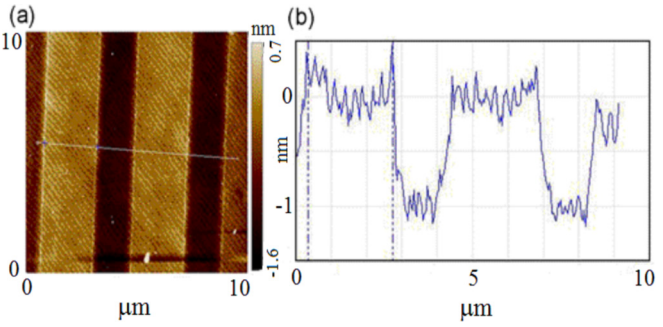

FIG. 2. (a) AFM image of LAO/STO sample S4, patterned with conducting stripes (brighter) spaced by insulating areas (darker). (b) Section profile height of the patterned stripes along the white line in (a). The conductive stripes are 2.4 μm wide, the spacing is 1.6 μm, and the vertical step on the LAO surface is just 1 nm high.

modes of STO (at 87 cm^{-1} and 173 cm^{-1}, respectively, at 300 K), the weak phonon TO4 which appears below T_c at 437 cm^{-1}. In both panels, the increase in the low-frequency $R(\omega)$ for $T \to 0$, same as that reported in the literature [9] for bare STO, is caused by the TO1 softening. We modeled the complex dielectric function by the usual expression for STO [20,21]

$$\widetilde{\epsilon}(\omega) = \epsilon_\infty \prod_j \frac{\left(\Omega_{LO}^2\right)_j - \omega^2 + i(\Gamma_{LO})_j\omega}{\left(\Omega_{TO}^2\right)_j - \omega^2 + i(\Gamma_{TO})_j\omega}. \qquad (2)$$

Here Ω_j and Γ_j are the central frequency and width of the jth longitudinal (LO) or transverse (TO) phonon, respectively. Once an analytic form for $\widetilde{\epsilon}(\omega)$ is available, one can calculate the real and imaginary parts of the complex refraction index [22]

$$n(\omega) = \tfrac{1}{2}\left(\epsilon_1 + \sqrt{\epsilon_1^2 + \epsilon_2^2}\right),$$
$$k(\omega) = \tfrac{1}{2}\left(-\epsilon_1 + \sqrt{\epsilon_1^2 + \epsilon_2^2}\right), \qquad (3)$$

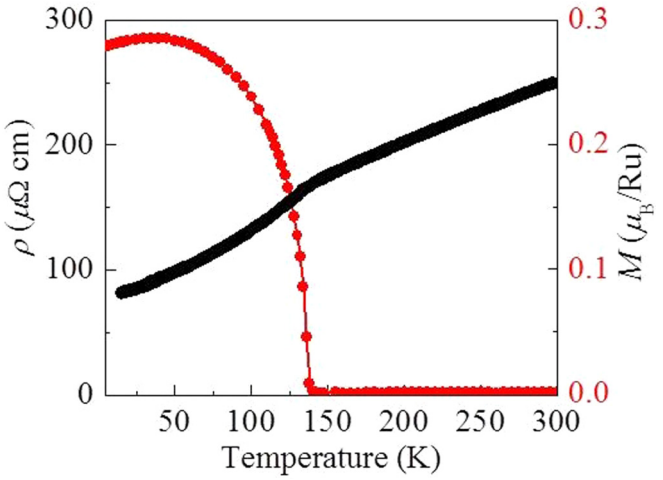

FIG. 3. Resistivity (black line, left scale) and magnetization (red dots, right scale) of the SRO film deposited on STO (sample S3). The red line is a guide to the eye.

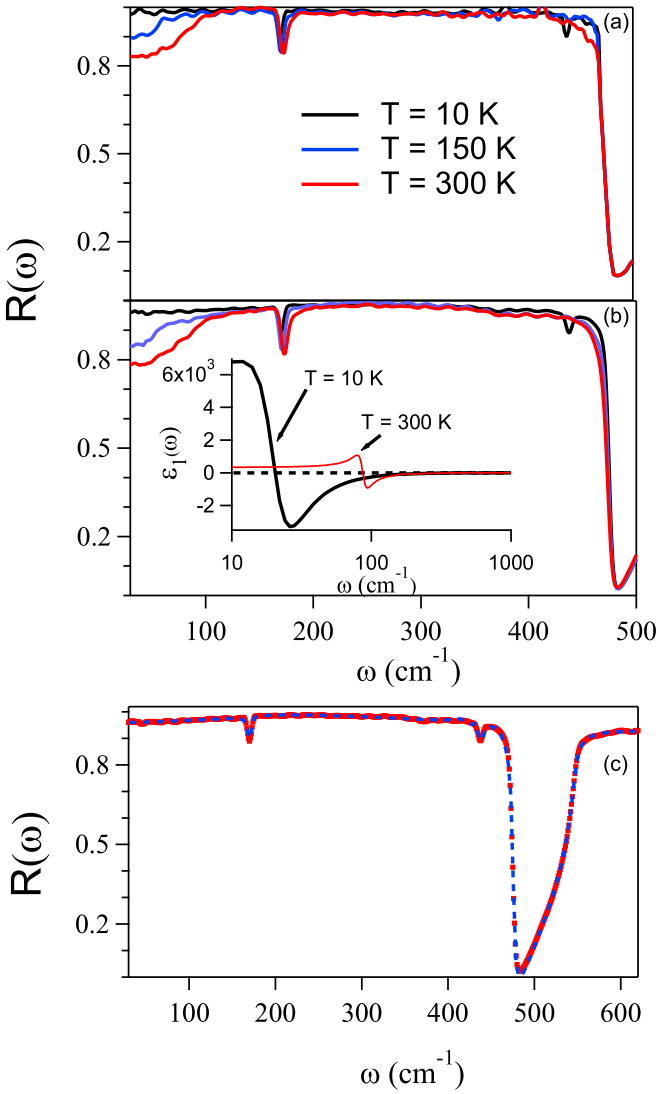

FIG. 4. Reflectivity of STO at different temperatures for the LAO/STO S1 sample (a), where the 2DES was erased by ion etching, and for the LAO/STO as-grown sample S2, which hosts the 2DES (b). (c) Best fit of Eq. (4) (dashed blue line) to the $R(\omega)$ of sample S1 at 10 K (red dots). The inset in (b) shows the $\epsilon_1(\omega)$ of sample S1 at 300 K (thin red line) and at 10 K (thick black line), as obtained from fits like that in (c).

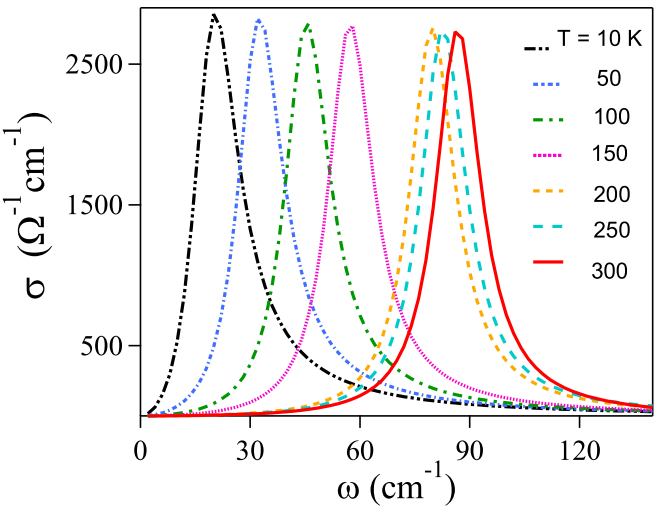

FIG. 5. Contribution to the optical conductivity of bulk STO by the soft mode TO1 in the LAO/STO sample S1.

which are finally inserted into the expression for the normal-incidence reflectivity of a semi-infinite medium

$$R(\omega) = \frac{(n-1)^2 + k^2}{(n+1)^2 + k^2}. \tag{4}$$

In doing so, we have assumed (i) that the LAO layer is transparent and provides no additional phase shift to the reflected wave and (ii) that the STO dielectric function is homogeneous within the penetration depth of the radiation in the sample, $\lambda_p \sim 1$ μm [17]. Equation (4) was fit to the experimental data using Ω_j and Γ_j ($j = 1,2,3$) as free parameters; below T_c we introduced a fourth LO-TO pair. An example of fit to data is reported in Fig. 4(c). The resulting values of the central frequencies and widths of the LO and TO modes are reported in Table II.

Figure 5 shows the contribution to the optical conductivity of the soft mode TO1 of bulk STO in the LAO/STO sample S1. Therein, both the oscillator strength and the width of TO1 are virtually independent of T, while its peak frequency Ω_{TO1} softens from 87 cm^{-1} at 300 K to 20 cm^{-1} at 10 K, in agreement within errors with previous determinations in bare STO [9]. Therefore, the normal-incidence reflectivity of LAO/STO can be hardly distinguished from that of bare STO. Moreover, no clear and reproducible difference could be obtained between the normal-incidence reflectivities of samples S1 and S2. Therefore, in order to detect a possible effect of the 2DES

TABLE II. Central frequency Ω and width Γ (in cm^{-1}) of the optical STO modes in the LAO/STO samples S1 and S2.

T (K)	LO1 Ω,Γ	TO1 Ω,Γ	LO2 Ω,Γ	TO2 Ω,Γ	LO3 Ω,Γ	TO3 Ω,Γ	LO4 Ω,Γ	TO4 Ω,Γ
10	169, 4	20, 14	476, 5	170, 4	798, 29	545, 24	475,3	437,17
50	170, 3	32, 16	476, 5	171, 2	797, 28	544, 24	475,3	437,17
100	170, 4	45, 18	476, 5	171, 4	797, 28	544, 24	475,3	437,17
150	170, 3	57, 18	476, 7	172, 3	797, 29	545, 24		
200	171, 3	80, 15	477, 7	172, 4	798, 30	545, 23		
250	172, 4	83, 11	476, 5	174, 4	798, 29	545, 24		
300	171, 4	87, 14	477, 7	173, 7	798, 29	545, 24		

on the TO1 phonon softening, more refined measurements were necessary. They will be described in Sec. III D.

B. Optical conductivity of the SRO/STO system

Figure 6(a) shows the reflectivity of the SRO/STO sample S3, where both the Drude-like absorption of its free carriers, and their screening effect on the STO phonons, are well evident. As the effect of screening is better understood in terms of the optical conductivity, we discuss our results in terms of this quantity instead of the dielectric function as for LAO/STO. Therefore, in order to obtain the $\sigma(\omega)$ of STO in this case, we considered multiple reflections in the double layer made by a metallic film (SRO) superimposed to a bulk insulator (STO), both of which are interfaced with a vacuum. The overall reflectivity was therefore written as [22]

$$R(\omega) = \left| \frac{\tilde{r}_m + \tilde{r}_{mi}\exp(i2\tilde{\delta}_m) + \tilde{r}_i\exp(i2(\tilde{\delta}_i+\tilde{\delta}_m)) + \tilde{r}_i\tilde{r}_{im}\tilde{r}_m\exp(i2\tilde{\delta}_i)}{1 + \tilde{r}_m\tilde{r}_{mi}\exp(i2\tilde{\delta}_m) + \tilde{r}_{mi}\tilde{r}_i\exp(i2\tilde{\delta}_i) + \tilde{r}_m\tilde{r}_i\exp(i2(\tilde{\delta}_i+\tilde{\delta}_m))} \right|^2. \quad (5)$$

In Eq. (5), $\tilde{r}$ is the Fresnel reflection coefficient at the vacuum-SRO (subscript m), SRO-STO (mi), and STO-vacuum (i) interface; $\tilde{\delta}$ is the optical retardation of the electric field when it propagates through the metallic film (subscript m) and through STO (i). The coefficients $\tilde{\delta}$ and $\tilde{r}$ are defined through the thickness $d_{m(i)}$ of SRO (STO), and through their refractive indexes $\tilde{n}_m(\omega)$ and $\tilde{n}_i(\omega)$. The former one was taken from Ref. [23], the latter one from the dielectric function $\tilde{\epsilon}_i(\omega)$, once modeled by the Drude-Lorentz expression

$$\tilde{\epsilon}(\omega) = \epsilon_\infty + \sum_j \frac{S_j^2}{(\omega^2 - \Omega_j^2) + i\Gamma_j\omega}. \quad (6)$$

A least-square procedure applied to Eqs. (5) and (6) provided the best values for S_j, Ω_j, and Γ_j ($j = 1, 2, 3$) for SRO/STO. Examples of such fits are reported In Fig. 6(a). A reliable value for the thickness of the conducting layer ($d \simeq 7$ nm) was also obtained. The central frequencies and widths of the first three TO phonons are reported in Table III. In SRO/STO, the weak TO4 mode is fully shielded.

As one can see in Fig. 6(b), which shows the line shapes of TO1 at different temperatures, at 10 K the TO1 phonon peak is much broader, and the peak frequency is appreciably higher, than for the STO covered by an insulating layer of Fig. 5. In SRO/STO at 10 K, $\Omega_{TO1} = 34\ \mathrm{cm}^{-1}$, corresponding to a hardening of $14\ \mathrm{cm}^{-1}$ with respect to bare STO (compare Table III with Table II). Such a low-temperature hardening of TO1 in the absence of a static field was not reported before in STO crystals, possibly because the metal electrodes were too thick to be semitransparent in the terahertz range. This effect is therefore novel for bulk STO under $\vec{E}_0 = 0$, and its extent is comparable with that observed in STO crystals under a static field $\vec{E}_0$ as high as 40 kV/cm parallel to the surface [12]. Notice that the electric field amplitude associated with both the blackbody and synchrotron IR radiation used in the present experiment is negligible, being lower than the $\vec{E}_0$ of Ref. [12] by several orders of magnitude.

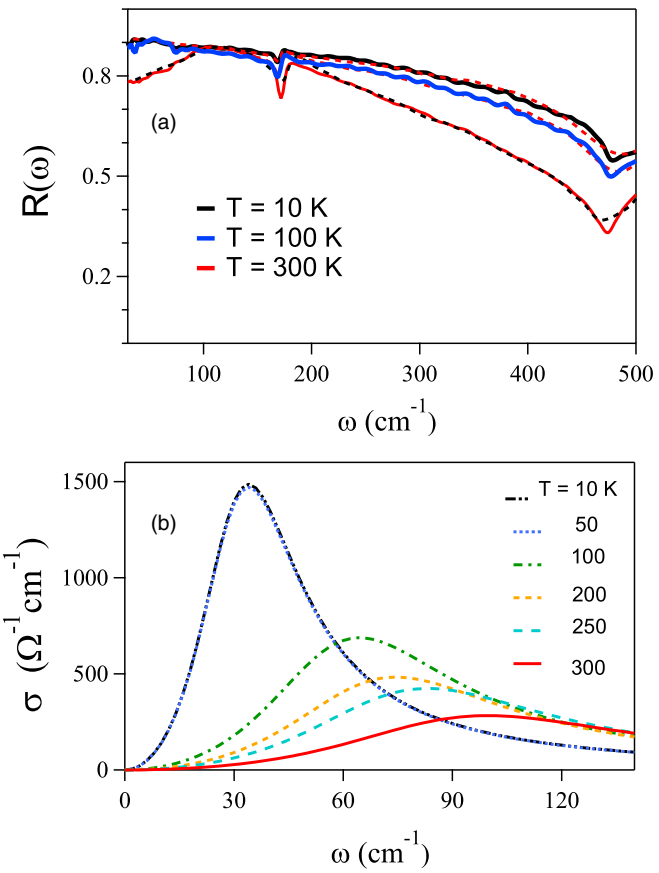

FIG. 6. (a) Reflectivity of the SRO/STO sample S3 at three temperatures (solid lines) and fits to data by use of Eq. (5) (dashed lines). (b) Contribution to the optical conductivity of the soft mode TO1 of bulk STO in the SRO/STO sample S3.

TABLE III. Central frequency Ω and width Γ (in cm^{-1}) of the transverse optical modes of STO observed in sample S3, as obtained from Eq. (6).

T (K)	TO1 Ω,Γ	TO2 Ω,Γ	TO3 Ω,Γ
10	34, 69	171, 2	514, 77
50	45, 61	171, 4	518, 84
100	62, 110	172, 5	540, 67
200	66, 36	173, 5	528, 50
250	80, 17	174, 6	522, 26
300	87, 34	176, 7	522, 53

C. Phonon hardening in bulk $SrTiO_3$ by a conducting layer at its surface

The change observed here in the TO1 frequency, and consequently in the STO permittivity through Eq. (1), points toward the existence of a dynamic depolarizing field $E_{\rm dep}$ close to the SRO/STO interface. At variance with the static field of Ref. [12], here $E_{\rm dep}$ fluctuates around Ω_{TO1}, as it is produced by the free electrons of SRO which follow adiabatically the anharmonic TO1 vibration. At any time, a dipole moment opposite to that within STO thus appears. It is parallel to the surface like that associated with the Ti-O cage motion, which is excited by the radiation field $\vec{E}(\omega)$ parallel to the interface. Therefore, the electron displacements have a high depolarization efficiency on the underlying STO planes. Here, there is a similarity with the static depolarization, which is more efficient for external fields parallel to the STO surface [12]. We infer from our data that the dynamic $E_{\rm dep}$ lowers the relative weight of the anharmonic terms in the interatomic potential, making the resulting potential well somewhat closer to that of a harmonic mode. This effect increases the TO1 phonon frequency in the STO planes closer to the interface with the metal, which experience a stronger depolarizing field. In order to check if this model may quantitatively explain our observations, we have adapted to the present case the approach of Zhou and Newns [5], who calculated the effective permittivity $\epsilon_1(0,z)$ of a generic ferroelectric between two metal electrodes, as a function of the distance z from the metal surface, in the absence of external fields. They found that $\epsilon_1(0,z)$ grows from very small values at $z \simeq 0$, up to its bulk value (for large z), according to [5]

$$\epsilon_1(0,z) \simeq \frac{T_1}{T + T_0/(z\lambda) - T_c}, \tag{7}$$

In STO, for the parameters T_0, T_1, and λ, the authors report 2060 K, 1.01×10^5 K, and $0.33 \div 1.0$ nm^{-1}, respectively. As STO never becomes ferroelectric, we can assume $T_c = 0$ thus eliminating the divergence that would occur in a true ferroelectric at a critical thickness z_c. With the above values of T_0 and T_1, and with $\lambda = 0.5$ nm^{-1} we obtain the curves reported in Fig. 7(a). Therein, both at 300 K and 10 K, $\epsilon_1(0,z)$ tends asymptotically to values (330 and 6500, respectively) in excellent agreement with those extracted from the reflectivity of the LAO/STO sample S1 [see Fig. 4(b)], which is in fact equivalent to bare STO. According to Eq. (1), any STO thin layer at z will thus contribute to the observed conductivity with a TO1 peak at

$$\Omega_{TO1}(z) = \prod_{j=1}^{3} \Omega_{LOj} \frac{\sqrt{\epsilon_\infty}}{\Omega_{TO2}\Omega_{TO3}\sqrt{\epsilon_1(0,z)}}. \tag{8}$$

In the right member of Eq. (8), $\epsilon_1(0,z)$ is that in Fig. 7(a), $\epsilon_\infty = 5.6$, and the frequencies are taken from Table II. The prediction of Eq. (8) is plotted in Fig. 7(b), which shows how the TO1 frequency increases when approaching the interface. The divergence for $z \to 0$ is interrupted at the highest $\Omega_{TO1}(z)$ observed in STO at high T (about 90 cm^{-1}). For $z \to \infty$, $\Omega_{TO1}(z)$ tends to 20 cm^{-1}, the value measured in sample S1 at 10 K. The superposition of contributions from layers at increasing z explains the broadening of the TO1 line observed for SRO/STO in Fig. 6(b). By integrating on z Eq. (8), up to the penetration depth of the THz radiation around Ω_{TO1} at 10 K ($\lambda_p = 250$ nm) one obtains $\langle\Omega_{TO1}\rangle = 35$ cm^{-1}, in excellent agreement with the best-fit peak frequency at 10 K in Table III (34 cm^{-1}).

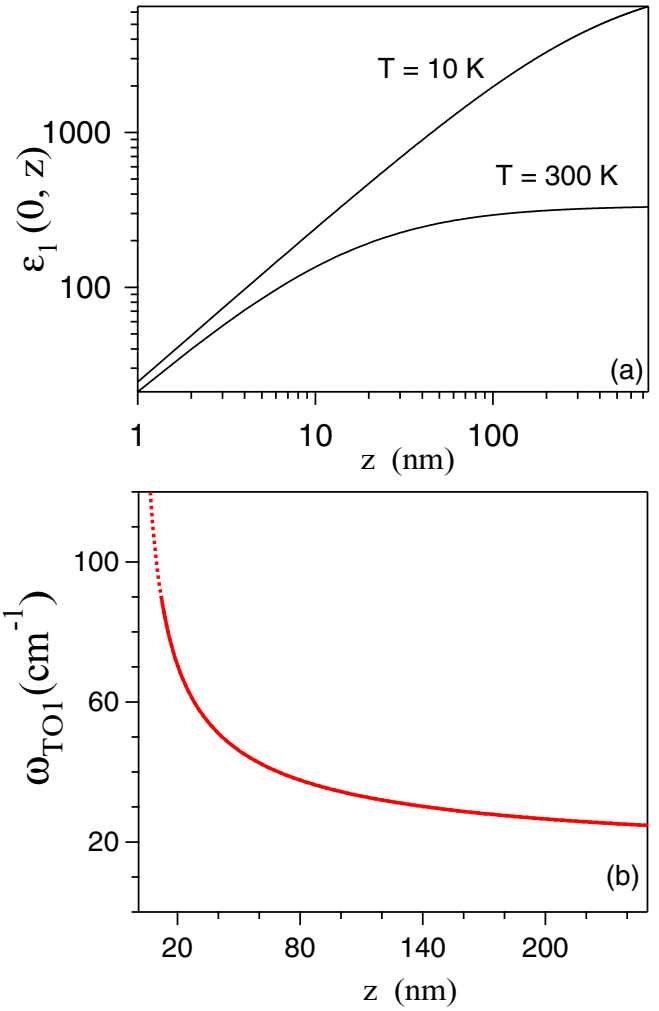

FIG. 7. (a) Permittivity of STO under the SRO film, calculated from Eq. (7) at two temperatures, vs the distance z from the metallic SRO layer on its surface, in the range of the THz radiation penetration depth in SRO/STO $\lambda_p = 250$ nm. (b) Resulting soft-mode frequency from Eq. (8) at 10 K. The solid line produced by the model, which diverges for $z \to 0$, has been stopped at the maximum Ω_{TO1} really observed in STO.

D. Detection of phonon hardening in microstriped LAO/STO

By taking into account what we learned on the interaction between STO and a thin film containing a conventional three-dimensional electron system, we can now reconsider the effect of the 2DES on the vibrational dynamics of STO. In principle, one could expect from the 2DES a depolarization effect similar to that generated by the metal thin film. However, such effect could not be observed in the reflectivity of Fig. 4(b). Possible reasons are a lower total number of electrons in the 2DES and/or the anisotropy of its conductivity tensor. With the aim of revealing this weaker effect, we increased the sensitivity of

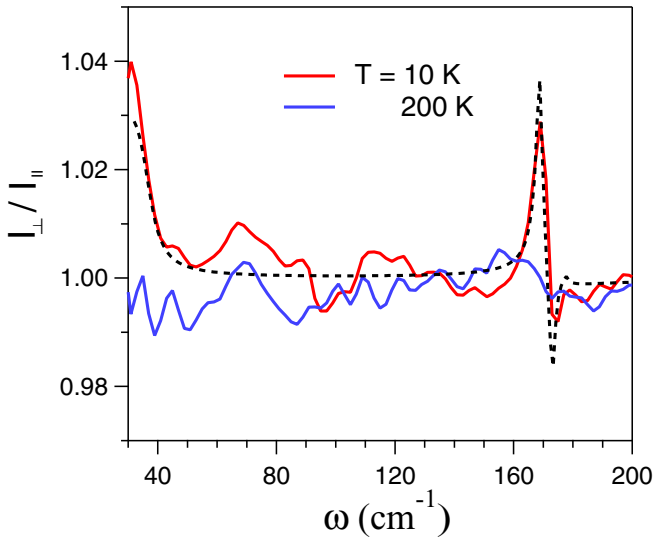

FIG. 8. Dichroic ratio $I_\perp/I_\parallel$ between the intensities reflected by the striped sample S4 when the radiation field $\vec{E}(\omega)$ is polarized orthogonal to the stripes and parallel to the stripes, at two temperatures. The dashed line is a fit to data based on Eq. (2).

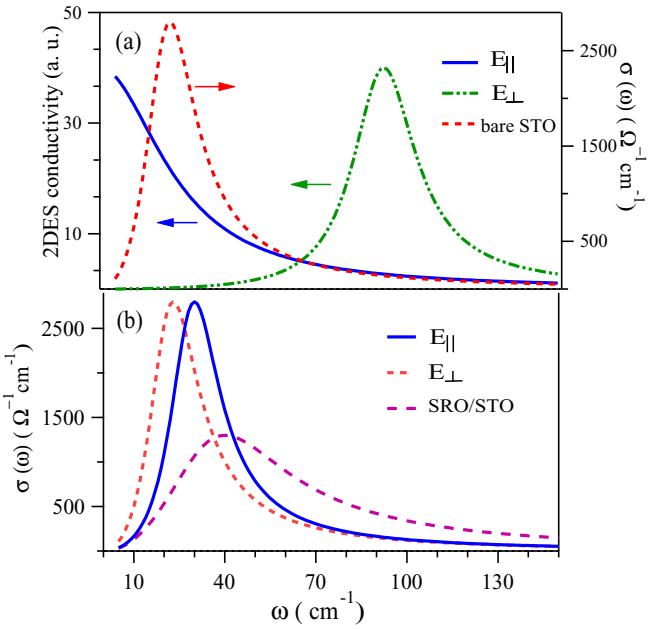

FIG. 9. (a) 2DES-model optical conductivity calculated for the THz field polarized parallel (blue solid line) and orthogonal (green dash-dotted line) to the stripes of sample S4. For comparison, the TO1 line of sample S1 at 10 K is reproduced from Fig. 5 (red dashed line). (b) The TO1 peak in $\sigma(\omega)$, measured with $\vec{E}_\perp$, and similar to that in bare STO, is compared: (i) with the TO1 conductivity for $E_\parallel$ reconstructed from the fit in Fig. 8, blueshifted by 7 cm^{-1} (solid line); (ii) with the phonon observed in the SRO/STO sample S3, from Fig. 6(b) (dashed line).

our experiment by using a linear dichroic setup on the striped sample S4. In the patterned sample one can decompose the dielectric response function into two independent components, the one probed by $\vec{E}(\omega)$ parallel to the stripes ($\vec{E}_\parallel$) and that probed by $\vec{E}(\omega)$ orthogonal to the stripes ($\vec{E}_\perp$). The linear dichroic intensity ratio $I_\perp/I_\parallel$ is shown in Fig. 8 at 200 K and 10 K in the THz range. At the highest temperature, $I_\perp/I_\parallel$ is independent of frequency within the experimental noise, whose amplitude is about 0.5% rms. This indicates that at 200 K both the TO1 and TO2 phonon frequencies, and their line shapes, are independent of the polarization. At 10 K instead, two sharp features appear at the TO1 and TO2 frequencies, demonstrating that both are blueshifted in $I_\parallel$ with respect to those measured in $I_\perp$. A fit to $I_\perp/I_\parallel$ based on Eq. (2) (dashed line in Fig. 8) provides a shift of 7 cm^{-1} for TO1, of 3 cm^{-1} for TO2. This result, which has been verified by a test reported in the Supplemental Material [19], can be interpreted in the following way.

It has been shown [24–26] that the THz conductivity of a 2DES patterned into stripes, or ribbons, of width W much smaller than both their length and the radiation wavelength, can be represented by a Drude peak when probed by $E_\parallel$, and by a Lorentzian peak when probed by $E_\perp$. The latter one has the same intensity and width as the Drude peak and is centered [24,27] at the standing-wave frequency ω_P of the confined plasmon polariton, given by

$$\omega_P = \sqrt{\frac{e^2 N_{2D}}{m^* \bar{\epsilon}_\infty} \frac{\pi}{W}}, \tag{9}$$

where N_{2D} is the charge density, m^* the electron effective mass, and $\bar{\epsilon}_\infty$ is an average, high-frequency value of $\epsilon_1(\omega)$. In the present case, $W = 2.4$ μm, $m^* = 0.9 m_e$ [28], and [17] $N_{2D} \simeq 10^{13}$ cm^{-2}, while for $\bar{\epsilon}_\infty$ we averaged the $\epsilon_\infty = 5.6$ of STO with the dielectric constant of a vacuum, as the plasmon field extends in both half-spaces above and below the 2DES. We thus obtained $\omega_P = 93$ cm^{-1}, by neglecting the small contribution to $\epsilon_1(\omega)$ of the weak phonons at frequencies higher than ω_P. The resulting conductivity of the 2DES $\sigma(\omega)$, where for both the Drude and Lorentz peaks we assumed a 25 cm^{-1} linewidth compatible with mobility values measured [17] at low T, is shown in Fig. 9(a). Therein, the Drude peak in $\sigma_\parallel(\omega)$ has a strong spectral weight in the soft-mode frequency range, suggesting that its free carriers can produce the dynamic depolarization field which, similar to those of SRO, increases the TO1 frequency, and decreases the permittivity. A reconstruction of the phonon mode conductivity in LAO/STO, shifted by 7 cm^{-1} with respect to that measured with $\vec{E}_\perp$ (dotted line) and consistent with the fit to the ratio $I_\perp/I_\parallel$ shown in Fig. 8, is drawn by a solid line in Fig. 9(b). In the same figure, the SRO/STO mode TO1 is reported once again for comparison (long-dashed line). On the contrary, the plasma oscillations that dominate $\sigma_\perp(\omega)$ display their maximum spectral weight at a frequency higher than any possible value of Ω_{TO1} [dash-dotted line in Fig. 9(a)] and their overlap with TO1 is negligible. They are therefore unable to affect the softening of TO1, which in the polarization orthogonal to the stripes proceeds like in bare STO. Finally, the fact that also TO2 experiences a small shift in Fig. 8 can be understood by considering that the strong anharmonic potential of STO mixes the TO1 mode with the other ones.

IV. CONCLUSION

In conclusion, our terahertz reflectivity measurements on $SrTiO_3$ crystals interfaced both with a 10-nm-thick conventional metal ($SrRuO_3$) and with the comparably thick 2DES created by a film of $LaAlO_3$ have shown, in both systems, a measurable hardening of the TO1 soft mode of STO, at low temperature, with respect to bare STO. This effect is novel for STO in the absence of static external fields, as it affects bulk STO at least within the THz penetration depth ($\lambda_p \sim 250$ nm in SRO/STO, ~ 1 μm in LAO/STO). The observed hardening can be attributed to the depolarization action of the free electrons at or above the STO surface, which follow adiabatically the displacements of Ti-O cage with respect to the Sr lattice and thus partially shield the soft mode. In the case of SRO/STO this assumption allowed us to obtain, by adapting previous calculations of Zhou and Newns, a quantitative agreement with data. In the case of LAO/STO, a smaller phonon shift could be detected only in a sample where the 2DES was patterned in the form of stripes by selective ion etching. This allowed us to observe, in a linear dichroic experiment, the different behavior of TO1 when it is coupled to free electrons (THz field parallel to the stripes) or to plasmon polaritons confined within the stripes (THz field orthogonal to them). We thus also obtained indirect evidence of plasmon polaritons in the 2DES of LAO/STO, which can hardly be observed directly due to the strong absorption of the infrared-active modes in strontium titanate.

ACKNOWLEDGMENTS

This work has been supported by the Italian Ministry of University and Research through the PRIN project *OXIDE* and by the European Commission CALIPSO Programme (HZBPHOTONS_CALIPSO-140) for the access to the synchrotron facilities. We also wish to thank J. Lorenzana and M. Grilli for useful discussions.

[1] S. K. Kurtz, Trans. Am. Crystallogr. Assoc. **2**, 63 (1975).
[2] C. H. Ahn, K. M. Rabe, and J.-M. Triscone, Science **303**, 488 (2004).
[3] D. Lee, H. Lu, Y. Gu, S.-Y. Choi, S.-D. Li, S. Ryu, T. R. Paudel, K. Song, E. Mikheev, S. Lee, S. Stemmer, D. A. Tenne, S. H. Oh, E. Y. Tsymbal, X. Wu, L.-Q. Chen, A. Gruverman, and C. B. Eom, Science **349**, 1314 (2015).
[4] G. Shirane and Y. Yamada, Phys. Rev. **177**, 858 (1969).
[5] C. Zhou and D. M. Newns, J. Appl. Phys. **82**, 3081 (1997).
[6] K. A. Müller and H. Burkard, Phys. Rev. B **19**, 3593 (1979), and references therein.
[7] G. V. Belokopytov, Ferroelectrics **168**, 69 (1995).
[8] H. Vogt, Phys. Rev. B **51**, 8046 (1995).
[9] J. T. Devreese, S. N. Klimin, J. L. M. van Mechelen, and D. van der Marel, Phys. Rev. B **81**, 125119 (2010).
[10] Indeed TO1, whose symmetry is F_{2u} at high temperature, splits below T_c into an E_u doublet and an A_{2u} singlet, which at 5 K were resolved in hyper-Raman spectra only [11] at 7.8 and 16.5 cm^{-1}, respectively.
[11] A. Yamanaka, M. Kataoka, Y. Inaba, K. Inoue, B. Hehlen, and E. Courtens, Europhys. Lett. **50**, 688 (2000).
[12] V. Skoromets, F. Kadlec, C. Kadlec, H. Němec, I. Rychetsky, G. Panaitov, V. Müller, D. Fattakhova-Rohlfing, P. Moch, and P. Kužel, Phys. Rev. B **84**, 174121 (2011).
[13] A. A. Sirenko, G. Bernhard, A. Golnik, A. M. Clark, J. Hao, W. Si, and X. X. Xi, Nature (London) **404**, 373 (2000).
[14] P. Marsik, K. Sen, J. Khmaladze, M. Yazdi-Rizi, B. P. P. Mallett, and C. Bernhard, Appl. Phys. Lett. **108**, 052901 (2016).
[15] A. Ohtomo and H. Y. Hwang, Nature (London) **427**, 423 (2004).
[16] J. Mannhart and D. G. Schlom, Science **327**, 1607 (2010).
[17] A. Dubroka, M. Rössle, K. W. Kim, V. K. Malik, L. Schultz, S. Thiel, C. W. Schneider, J. Mannhart, G. Herranz, O. Copie, M. Bibes, A. Barthélémy, and C. Bernhard, Phys. Rev. Lett. **104**, 156807 (2010).
[18] P. P. Aurino, A. Kalabukhov, N. Tuzla, E. Olsson, T. Claeson, and D. Winkler, Appl. Phys. Lett. **102**, 201610 (2013).
[19] See Supplemental Material at http://link.aps.org/supplemental/10.1103/PhysRevB.93.224103 for details of the experimental procedure.
[20] F. Gervais, J.-L. Servoin, A. Baratoff, J. G. Bednorz, and G. Binnig, Phys. Rev. B **47**, 8187 (1993).
[21] K. Kamarás, K.-L. Barth, F. Keilmann, R. Henn, M. Reedyk, C. Thomsen, M. Cardona, J. Kircher, P. L. Richards, and J.-L. Stehlé, J. Appl. Phys. **78**, 1235 (1995).
[22] M. Dressel and G. Grüner, *Electrodynamics of Solids* (Cambridge University Press, Cambridge, UK, 2002).
[23] P. Kostic, Y. Okada, N. C. Collins, Z. Schlesinger, J. W. Reiner, L. Klein, A. Kapitulnik, T. H. Geballe, and M. R. Beasley, Phys. Rev. Lett. **81**, 2498 (1998).
[24] S. J. Allen, D. C. Tsui, and R. A. Logan, Phys. Rev. Lett. **38**, 980 (1977).
[25] L. Ju, B. Geng, J. Horng, C. Girit, M. Martin, Z. Hao, H. A. Bechtel, X. Liang, A. Zettl, Y. R. Shen, and F. Wang, Nat. Nanotechnol. **6**, 630 (2011).
[26] P. Di Pietro, M. Ortolani, O. Limaj, A. Di Gaspare, V. Giliberti, F. Giorgianni, M. Brahlek, N. Bansal, N. Koirala, S. Oh, P. Calvani, and S. Lupi, Nat. Nanotechnol. **8**, 556 (2013).
[27] V. Giliberti, A. Di Gaspare, E. Giovine, M. Ortolani, L. Sorba, G. Biasiol, V. V. Popov, D. V. Fateev, and F. Evangelisti, Phys. Rev. B **91**, 165313 (2015).
[28] A. McCollam, S. Wenderich, M. K. Kruize, V. K. Guduru, H. J. A. Molegraaf, M. Huijben, G. Koster, D. H. A. Blank, G. Rijnders, A. Brinkman, H. Hilgenkamp, U. Zeitler, and J. C. Maan, APL Mater. **2**, 022102 (2014).